

Análisis dinámico de impactos en sistemas mecánicos de topología variable

J.M. Font-Llagunes

Dpto. Ingeniería Mecánica. Universitat Politècnica de Catalunya
josep.m.font@upc.edu

J. Kövecses

Dept. Mechanical Engineering and Centre for Intelligent Machines. McGill University
jozsef.kovecses@mcgill.ca

Abstract

Mechanical systems with time-varying topology appear frequently in natural or human-made artificial systems. The nature of topology transitions is a key characteristic in the functioning of such systems. In this paper, a concept to decouple kinematic and kinetic quantities at the time of topology transition is used. This approach is based on the use of impulsive bilateral constraints (inert constraints) and it is a useful and elegant method for the analysis of energy redistribution and velocity change when these constraints are suddenly established. Two examples of variable topology mechanical systems are analyzed: a bipedal walking system and a dual-pantograph robotic prototype making contact with a stiff environment. For the first example, numerical simulations are presented to discuss the effects of configuration and design parameters on the dynamics and energetics of heel strike. For the second example, detailed experimental analysis is carried out to illustrate different concepts introduced in this work.

INTRODUCTION

Variable topology mechanical systems are present in various fields of application, e.g., robotics, biomechanics and mechanism science. The dynamic analysis of such systems depends on the time-varying nature of the constraints established between the elements of the multibody system and the environment. This fact complicates the analysis because in most cases a different dynamic model must be developed for each constraint configuration. Furthermore, constraints are usually established due to impacts which also require a different dynamics formulation to be characterized. Typical situations that occur in variable topology systems are:

- (1) The number of degrees of freedom of the system decreases via the development of certain connections. An example for this can be the grasping/capturing of a moving payload, which may also represent the interaction of two robotic mechanisms, or a human and a payload. The effect of mass capture on flexible multibody systems was studied in [1]. This group of problems includes two possibilities: the developed connections can exist for a finite period of time or they can represent an instantaneous situation only.
- (2) The constraint configuration is changing: some constraints are added and some become passive at the same time. In this case, the effective number of degrees of freedom may stay the same. An example for this situation can be found in the analysis of (active/passive) dynamic walking machines [2]. In those systems, the heel strike event represents a sudden change of topology where some constraints are imposed on the foot that makes contact, and other are released from the foot that leaves the ground [3, 4, 5].

Discontinuous constraints have been a known concept in analytical mechanics [6, 7]. Two particular cases of such discontinuous constraint configurations can be the sudden removal and the sudden addition of constraints. The sudden removal of constraints alone does not instantaneously change the energy and momentum distribution of the system unless other impulsive forces are exerted during the transition. The sudden addition of constraints does cause instantaneous changes. Therefore, the truly critical event during the motion of variable topology

systems is when physical connections are established. Such an event can be characterized by inert constraints, which are a class of bilateral impulsive constraints [6, 7].

This work focuses on this event and particularly on the effects of the system state (configuration and velocities) on various dynamic aspects of the transition. The dynamic analysis conducted in this work is based on an analytical approach that allows a complete decomposition of the dynamic equations and the kinetic energy to two subspaces of the tangent configuration space of the system, i.e., the spaces of constrained and admissible motions [8]. It will be shown that this approach is well-suited to better characterize topology transitions and get insight into the dynamic behavior of these systems during contact.

Two situations that can be characterized by means of inert constraints are studied in this paper. We focus first on the heel strike event of bipedal locomotion. This is a relevant event because it represents the main cause of energy consumption during the gait cycle [5]. Furthermore, it plays an important role to guarantee the cyclic stability of the motion. Human walking is not locally stable, but it is cyclically stabilized by the removal of energy that takes place at each heel strike. Different dynamic aspects of the heel strike are analyzed in this work, paying special attention on the energy redistribution at topology transition. The magnitude of the contact impulses developed on the foot are also calculated for different configurations and design parameters of a simple bipedal system: a compass-gait walker with circular feet and a torso.

The second example studied in the paper is the case of a robotic multibody mechanical system that makes contact with a stiff environment. An experimental testbed consisting of two dual-pantograph devices is used for that purpose. By means of it, detailed experimental analysis is carried out to illustrate different concepts introduced in this work.

DYNAMICS FORMULATION AND DECOMPOSITION

Let us consider that t_i represents a typical time for the change of topology where certain constraint conditions are suddenly imposed. This event takes place in the $[t_i^-, t_i^+]$ interval where t_i^- and t_i^+ represent the pre- and post-event instants, respectively. The duration of this interval can usually be considered very short on the characteristic time scale of the finite motion of the system. Therefore, in $[t_i^-, t_i^+]$ the configuration of the system is assumed to be constant. The event of topology change is characterized by m impulsive constraints, which can normally be written as

$$\mathbf{A}\mathbf{v}^+ = \mathbf{0}, \quad (1)$$

where \mathbf{v}^+ represents the $n \times 1$ array of generalized velocities at the post-event instant t_i^+ , and \mathbf{A} is the $m \times n$ constraint Jacobian matrix. These constraints represent the required topology at t_i^+ at the velocity level and they are also known as inert constraints [6, 7]. The general case where these constraints are realized either in an ideal or a non-ideal way is considered in this work.

These above impulsive constraints capture the physical conditions due to a sudden change in topology. A general approach can be developed based on them to characterize several aspects of the behavior of mechanical systems with varying topology. A key principle, we will also use here, is the principle of the relaxation of constraints that will allow us to turn the bilateral constraint conditions of Eq. (1) into the more general form of a mapping in the tangent space of the dynamic system [8]. This mapping will make it possible to interpret a decomposition in the tangent space.

The tangent space of the mechanical system can be seen as an n dimensional linear space that is interpreted for each configuration [9]. Since the configuration of the system is assumed to be constant during the topology change interval, a single representation of this linear space can be used. Via the relaxation of the impulsive constraints we obtain a mapping that can be interpreted for the two representative time instants as $\mathbf{A}\mathbf{v}^- = \mathbf{u}_c^-$ and $\mathbf{A}\mathbf{v}^+ = \mathbf{u}_c^+$. This mapping defines a subspace of the tangent space, the space of constrained motion (SCM). The subspace that complements the SCM to the whole tangent space is the space of admissible motion (SAM) [8]. The dynamics associated with the topology change primarily takes place in the SCM. Array \mathbf{u}_c contains velocities along the m representative directions of the SCM. Motion along these directions is constrained by the topology change, and $\mathbf{u}_c^+ = \mathbf{0}$ according to Eq. (1). Array \mathbf{u}_c may also be seen to give a local parameterization for the SCM [8].

The above two subspaces can be defined so that they are orthogonal to each other with respect to the natural, mass metric of the tangent space [8]. In that case, any impulsive event characterized by ideal impulsive

constraints of the form of Eq. (1) will influence quantities in the SCM, and will leave the SAM unaffected. However, non-ideal effects, like friction, can couple the two subspaces and develop an influence on the admissible motion dynamics too. The decomposition to the two subspaces can be accomplished via asymmetric projection operators. For the case when the constraints are linearly independent, i.e., the constraint Jacobian has a full row rank, the mentioned projection matrices can be obtained as [8]

$$\mathbf{P}_c = \mathbf{M}^{-1} \mathbf{A}^T (\mathbf{A} \mathbf{M}^{-1} \mathbf{A}^T)^{-1} \mathbf{A}, \quad (2)$$

$$\mathbf{P}_a = \mathbf{I} - \mathbf{M}^{-1} \mathbf{A}^T (\mathbf{A} \mathbf{M}^{-1} \mathbf{A}^T)^{-1} \mathbf{A}, \quad (3)$$

where \mathbf{I} is the $n \times n$ identity matrix, \mathbf{M} is the mass matrix of the system, and \mathbf{P}_c and \mathbf{P}_a are the mentioned projection operators. These are used to project kinematic quantities to the SCM and SAM, respectively, and their transposes project kinetic quantities [8]. It can be proved that the projectors above are orthogonal with respect to the mass matrix, i.e., $\mathbf{P}_c^T \mathbf{M} \mathbf{P}_a = \mathbf{P}_a^T \mathbf{M} \mathbf{P}_c = \mathbf{0}$.

By means of the decomposition presented above, the kinetic energy of the system, $T = (1/2) \mathbf{v}^T \mathbf{M} \mathbf{v}$, can be completely decoupled in two terms T_c and T_a associated with the SCM and the SAM, respectively. This kinetic energy decomposition can be represented as

$$T = T_c + T_a = \frac{1}{2} \mathbf{v}_c^T \mathbf{M} \mathbf{v}_c + \frac{1}{2} \mathbf{v}_a^T \mathbf{M} \mathbf{v}_a, \quad (4)$$

where $\mathbf{v}_c = \mathbf{P}_c \mathbf{v}$ and $\mathbf{v}_a = \mathbf{P}_a \mathbf{v}$.

Any force or impulse arising in the SCM will change only T_c leaving T_a unaffected. Also, any change of the generalized velocities that influences \mathbf{v}_c or \mathbf{v}_a only, will cause a change in T_c or T_a , respectively, while leaving the other unchanged. The impulsive event, with the assumption of ideal constraint realization, gives rise to generalized forces and impulses which will influence T_c only. In this case, T_c will be completely lost in the topology transition, $T_c^+ = 0$, and the total post-event kinetic energy will equal the pre-event kinetic energy of the SAM, $T^+ = T_a^-$.

The impulsive dynamic equations can be represented in the decoupled form as

$$\left[\frac{\partial T_c}{\partial \mathbf{v}_c} \right]^+ = \mathbf{M} (\mathbf{v}_c^+ - \mathbf{v}_c^-) = \mathbf{A}^T (\bar{\boldsymbol{\lambda}} + \bar{\boldsymbol{\Lambda}}), \quad (5)$$

which gives the impulse-momentum level dynamic equations for the SCM, and

$$\left[\frac{\partial T_a}{\partial \mathbf{v}_a} \right]^+ = \mathbf{M} (\mathbf{v}_a^+ - \mathbf{v}_a^-) = \mathbf{P}_a^T \bar{\mathbf{f}}_N, \quad (6)$$

represents the dynamics of impulsive motion for the SAM. In Eqs. (5) and (6), $\bar{\boldsymbol{\lambda}}$ and $\bar{\boldsymbol{\Lambda}}$ represent the impulses of the generalized constraint and non-ideal forces associated with the local parameterization, \mathbf{u}_c , of the SCM. The impulses of the generalized non-ideal forces can usually be expressed with force laws such as $\bar{\mathbf{f}}_N = \bar{\mathbf{f}}_N(\bar{\boldsymbol{\lambda}}, \mathbf{v}, \mathbf{q})$ (e.g., friction). They can then be projected to the subspaces and included in the above impulsive dynamic equations as $\mathbf{P}_c^T \bar{\mathbf{f}}_N$ and $\mathbf{P}_a^T \bar{\mathbf{f}}_N$, respectively. For the SCM the associated generalized impulse component can be expressed as $\mathbf{P}_c^T \bar{\mathbf{f}}_N = \mathbf{A}^T \bar{\boldsymbol{\Lambda}}$. In the case of ideal constraint realization, only $\bar{\boldsymbol{\lambda}}$ is present in the above equations ($\bar{\mathbf{f}}_N = \mathbf{0}$). However, in general, the magnitudes of the elements of $\bar{\boldsymbol{\lambda}}$ are different for ideal and non-ideal realizations [8].

The detailed analysis of the formulation outlined can provide important tools to analyze and design variable topology systems and gain deeper insight into their behavior. We can develop a thorough understanding and description on the energy redistribution and momentum transfer at topology change. In turn, this makes it possible to gain insight, develop performance measures, and guidelines for the design of variable topology mechanical systems and their control. It is noteworthy that the approach described does not require the assumption of idealistic topology transitions. Effects of non-ideal phenomena (such as friction) can be considered.

APPLICATION EXAMPLES

We will use numerical and experimental results obtained for two variable topology systems to illustrate the usefulness of the previous approach. The first is the model of a compass-gait biped with torso, Fig. (1a). This system changes its topology at each heel strike, which can be realistically modeled with ideal impulsive constraints. Based on the proposed formulation, we study the effects of various design parameters on the dynamics of the topology change and illustrate the capabilities of the approach.

The second example includes an experimental multibody system, Fig. (1b). The passive device emulates a stiff environment with a flat surface and the active device comes to a contact interaction with the passive one. This is the case of a general impact situation where the topology change lasts only for a very short period of time. The compression phase associated with this interaction represents a topology transition and can be modeled with impulsive constraints. Non-ideal phenomena, such as friction, are also present in this case and cannot be neglected in general. We will use the data obtained via performing several sets of experiments for different pre-impact conditions. Based on this, we will illustrate how the proposed decomposition approach can be used to represent the intensity of topology transitions and provide dynamics performance characterization.

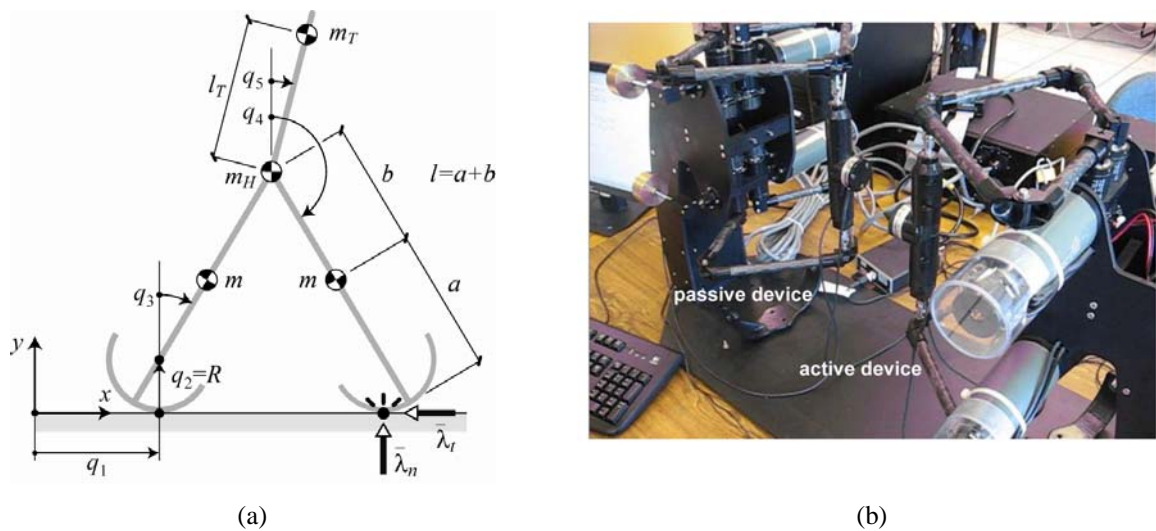


Fig. 1. Application examples: (a) Compass-gait biped with torso, (b) Experimental setup with two Quanser dual-pantograph devices.

Example 1: Numerical analysis of heel strike dynamics of a compass-gait biped with torso

In bipedal locomotion, the constraint configuration imposes that the swing foot stays in contact with the ground without slipping after heel strike, i.e., the velocity of the contact point becomes zero after impact. This is the desired situation in walking motion, which can be expressed by bilateral impulsive constraints of the form of Eq. (1) [10]. After heel strike, the swing foot changes its role and becomes the stance foot of the next step. We assume that non-ideal effects are not present in this situation.

We will analyze the heel strike event of a compass walker with circular feet and torso, Fig. (1a). It consists of two identical legs of length l and mass m . The center of mass (COM) of each leg is at a distance b from the hip. The radius of the feet is R and the hip is modeled as a point mass m_H located at the revolute joint between the legs. The torso is included as a third link that can rotate about the hip with mass m_T and the center of mass located at a distance l_T from the hip. The value of the fixed parameters is given in Table (1).

We define two dimensionless parameters which will be varied to investigate its dynamic effects. These are $\rho = R/l$, which establishes a relationship between the foot radius and the length of the leg, and $\mu = m_T/2m$, which accounts for the mass distribution between upper and lower body.

Table 1. Dynamic parameters of the bipedal walking system.

Parameter	Value	Description
m_W	30 kg	Total mass of the walking system
m_H	10 kg	Mass of the hip
l	0.8 m	Length of the leg ($l = a + b$)
b	0.4 m	Position of the COM of the leg
l_T	0.4 m	Position of the COM of the torso

The configuration of the compass walker can be described by the 5 generalized coordinates q_i ($i=1,\dots,5$) shown in Fig. (1a). The time derivatives of these coordinates define the vector of generalized velocities \mathbf{v} . For the system at hand, we obtained the mass matrix \mathbf{M} and the Jacobian \mathbf{A} associated with the constraints established at heel strike. As mentioned before, these constraints establish that the velocity of the contact point goes to zero at heel strike.

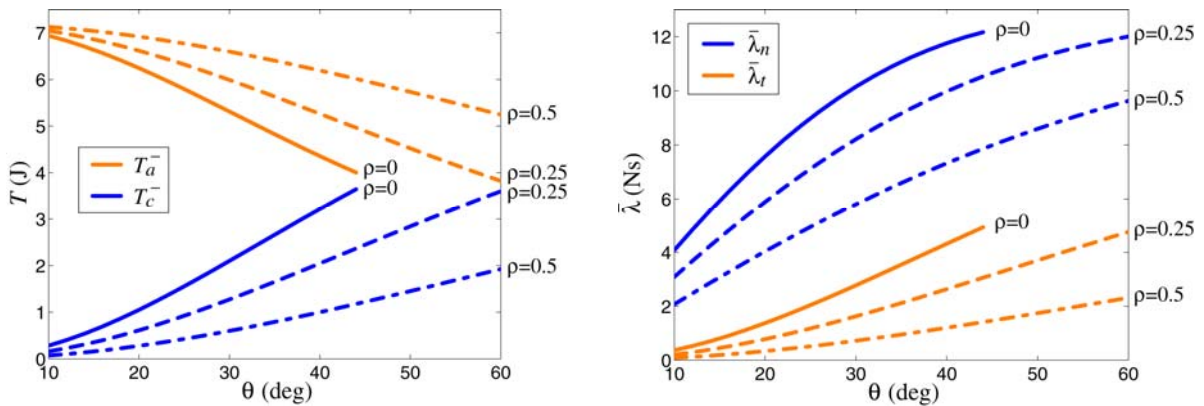
The dynamic analysis of topology change is based on the pre-impact velocities \mathbf{v}^- . To obtain this vector the following assumptions were made for the pre-impact kinematics:

- (1) The stance foot rolls over the ground without slipping, $\dot{q}_1^- = R\dot{q}_3^-$ and $\dot{q}_2^- = 0$.
- (2) The upper body does not rotate with respect to the absolute inertial frame, $\dot{q}_5^- = 0$.
- (3) Both legs rotate with an angular velocity of 1 rad/s with respect to the absolute inertial frame, $\dot{q}_3^- = \dot{q}_4^- = 1$ rad/s. These are typical values for compass-gait walkers [11].

Based on those, we obtained the pre-impact kinetic energy decomposition and the impulses developed on the contact point $\bar{\lambda} = [\bar{\lambda}_r, \bar{\lambda}_t]^T$, Fig. (1a), for different configurations and designs.

We analyze first the influence of the foot radius R and the angle θ between the legs on the dynamics of heel strike. Note that angle $\theta = 2q_3$ at heel strike. We consider the following interval of possible angles: $\theta \in [10^\circ, 60^\circ]$. As for the configuration of the upper body, we assume that it is placed perpendicular to the ground at impact. The effect of the foot radius design is analyzed considering the following values of ρ : 0, 0.25, and 0.5. The parameter representing the mass distribution is $\mu = 1$.

Fig. (2) shows the kinetic energy decomposition just before heel strike and the magnitude of impulses developed as functions of θ for the considered values of ρ . The pre-event energy decomposition is useful because it indicates the energy which will be lost during topology change (T_c^-) and the energy that will remain in the system after the transition ($T_a^- = T_a^+$).


 Fig. 2. Kinetic energy decomposition and impulses at contact point as functions of θ and ρ .

Several conclusions can be drawn based on the results shown in Fig. (2). First, it can be seen that the larger the foot radius is, the lower the energetic losses are at heel strike. Also, for a given foot radius, a low inter-leg angle θ provides lower energetic losses. It can be also seen that a point-foot walker ($\rho = 0$) is clearly less efficient than a circular-feet walker ($\rho > 0$), which is in complete agreement with [12]. The curve for $\rho = 0$ does not cover all the range of angles because for $\theta > 43^\circ$ the stance foot does not lift up from the ground after heel strike and, therefore, forward motion is not obtained.

Regarding the impulses $\bar{\lambda}_n$ (normal direction) and $\bar{\lambda}_t$ (tangential direction), Fig. (2) shows that both of them grow with θ and decrease with ρ . The point-foot walker is the one that yields higher impulses for a given angle (in both directions). It can be shown that high contact impulses are obtained when T_c^- is also high.

Secondly, we analyze how the torso orientation and the walker mass distribution affect the dynamics of heel strike. For this purpose, we study impacts for a usual inter-leg angle $\theta = 40^\circ$, and a fixed foot radius $R = 0,25l$ (i.e., $\rho = 0,25$). The influence of the configuration of the torso is analyzed by varying angle q_5 within the range $[-20^\circ, +20^\circ]$. That is, configurations between upper body leaning backward aligned with the front leg ($q_5 = -20^\circ$) and upper body leaning forward aligned with the rear leg ($q_5 = +20^\circ$). As for the mass distribution, its effects are studied by considering the following values of μ : 0.1, 1, and 10.

Fig. (3) represents the kinetic energy decomposition and the magnitude of the developed impulses as functions of q_5 for the considered values of the mass distribution ratio μ . Based on the obtained results, it can be seen that a body posture with the torso leaning forward is better to minimize energetic losses (lower T_c^-). Such an angle also increases T_a^- , which is the energy that will stay in the system after topology transition. The mass distribution of the walker (parameterized with μ) has different consequences depending on the torso angle. It can be seen that for negative q_5 a low value of μ is better to reduce energy losses, whereas for positive q_5 a high value of μ works better in terms of energetic efficiency.

According to the results, a good guideline to obtain less consuming heel strike transitions in humanoid robotics would be to place the torso slightly leaning forward. It is worth noting that this conclusion is also supported by [13], in which the complete gait of a compass-gait walker with upper body was optimized. The obtained optimal joint-angle evolution shows an upper body configuration inclined forward aligned with the non-colliding leg at the end of the gait (heel strike). From the results obtained, it can also be concluded that it is advisable to design robots with the mass more concentrated in the torso than in the legs ($\mu > 1$). As before, it can be shown that the magnitude of the contact impulses is correlated with T_c^- . Therefore, the last considerations given to reduce energy losses also hold if we want to obtain lower contact impulses.

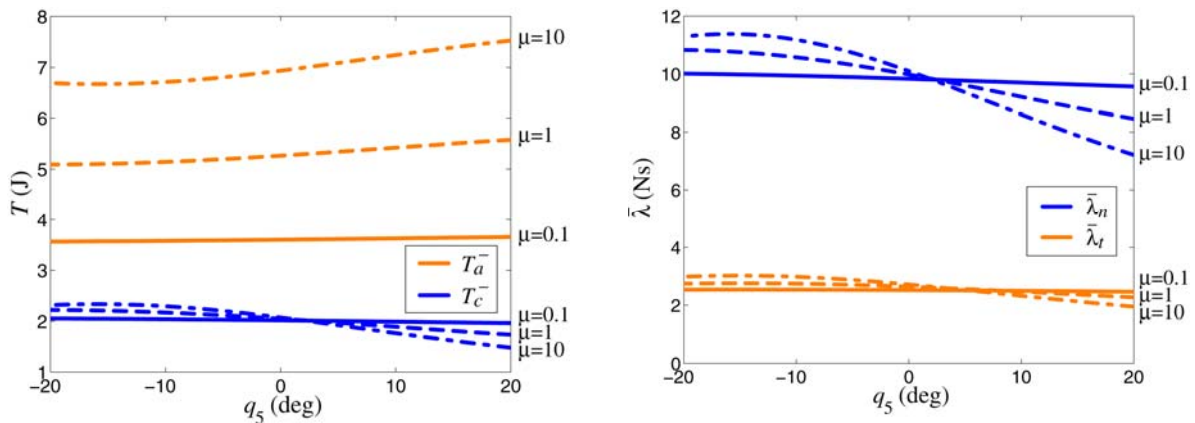


Fig. 3. Kinetic energy decomposition and impulses at contact point as functions of q_5 and μ .

Example 2: Experimental analysis of contact interaction between two robotic systems

An experimental testbed based on two dual-pantograph devices has been used to investigate the presented concepts. The real system is shown in Fig. (1b). Each device is equipped with high-resolution force/torque sensors at the tip and optical encoders at the motor joints. In the experiments one of these devices (passive

device) emulates a stiff environment with a flat surface and the other (active device) comes to a contact interaction with the passive one at one single contact point. The compression phase of this interaction represents a topology transition that can be modeled with impulsive constraints of the form of Eq. (1).

The trajectories performed have been programmed so that the motion of the system can be considered planar. The planes of the two pantographs are parallel so they can be considered with one single “composite” pantograph model, see Fig. (4a). In this figure, angles q_i denote the absolute orientation of the i th link ($i=1,2,3,4$) of the pantograph. Regarding the parameters, l_i and a_i represent the length and the position of the center of mass of the i th link, m_i and I_i denote its mass and moment of inertia about its center of mass, and m_{EE} denotes the mass of the end effector. Parameter l_5 indicates the distance between the two actuation motors. The value of these parameters can be found in Table (2).

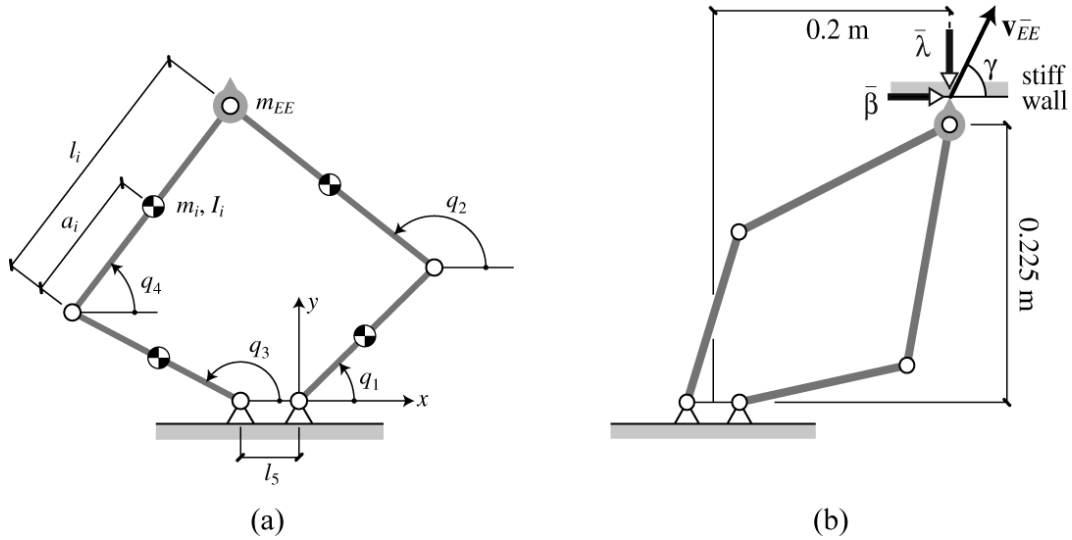


Fig. 4. (a) Planar dynamic model of the pantograph, (b) Considered contact configuration.

Table 2. Dynamic parameters of the pantograph.

Parameter	Value	Description
l_1, l_3	0.1449 m	Length of links 1 and 3
l_2, l_4	0.1984 m	Length of links 2 and 4
a_1, a_3	0.0519 m	Position of the COM of links 1 and 3
a_2, a_4	0.1081 m	Position of the COM of links 2 and 4
l_5	0.0445 m	Distance between axes of actuated joints
m_1, m_3	0.1202 kg	Mass of links 1 and 3
m_2, m_4	0.1084 kg	Mass of links 2 and 4
m_{EE}	0.3144 kg	Mass of the end effector
I_1, I_3	0.0004 kgm ²	Moment of inertia of links 1 and 3
I_2, I_4	0.0007 kgm ²	Moment of inertia of links 2 and 4

For planar motion, the system can be considered as a 2-DOF mechanism and the actuated joint coordinates $\mathbf{q} = [q_1, q_3]^T$ and their time derivatives $\dot{\mathbf{q}} = \mathbf{v}$ may be used as independent generalized coordinates and velocities, respectively. Using this representation, the mass matrix \mathbf{M} and the constraint Jacobian \mathbf{A} have been determined. The topology transition can be represented with one impulsive constraint that describes the sudden imposition of the physical contact constraint on the end point of the active device along the y direction.

We have performed four sets of experiments for the asymmetric configuration shown in Fig. (4b), these are named cases 1 to 4. Different situations have been tested by varying the angle γ of the pre-event velocity vector of the end effector, $\mathbf{v}_{EE}^- = [\dot{x}_{EE}^-, \dot{y}_{EE}^-]^T$, with respect to the tangential direction of the contact (see Fig. (4b)). The velocities and expected values of T_c^- , T_a^- , and $\xi = T_c^-/T^-$ are shown in Table (3). The magnitudes of the velocities have been determined imposing that the total $T^- = 10$ mJ. Note that for this configuration $\xi = 1$ (i.e., all the pre-impact kinetic energy contained in the SCM) does not correspond to having a velocity of the end point perpendicular to the wall. In fact, this is obtained when the angle of the velocity with respect to the tangential direction is $\gamma = 97.58^\circ$. This issue is addressed and further expanded in [14], where an eigenvalue problem is formulated to determine the directions associated with $\xi = 0$ and 1.

Table 3. Computations for the four considered velocities.

Case	γ	$\ \mathbf{v}_{EE}^-\ $ (m/s)	T_c^- (mJ)	T_a^- (mJ)	ξ
1	97.58°	0.1955	10	0	1
2	90°	0.1921	9.82	0.18	0.98
3	75°	0.1857	8.57	1.43	0.86
4	60°	0.1812	6.56	3.44	0.66

Each experiment has been performed several times and the results averaged. The results for the kinetic energy decomposition during one individual impact are shown in Fig. (5).

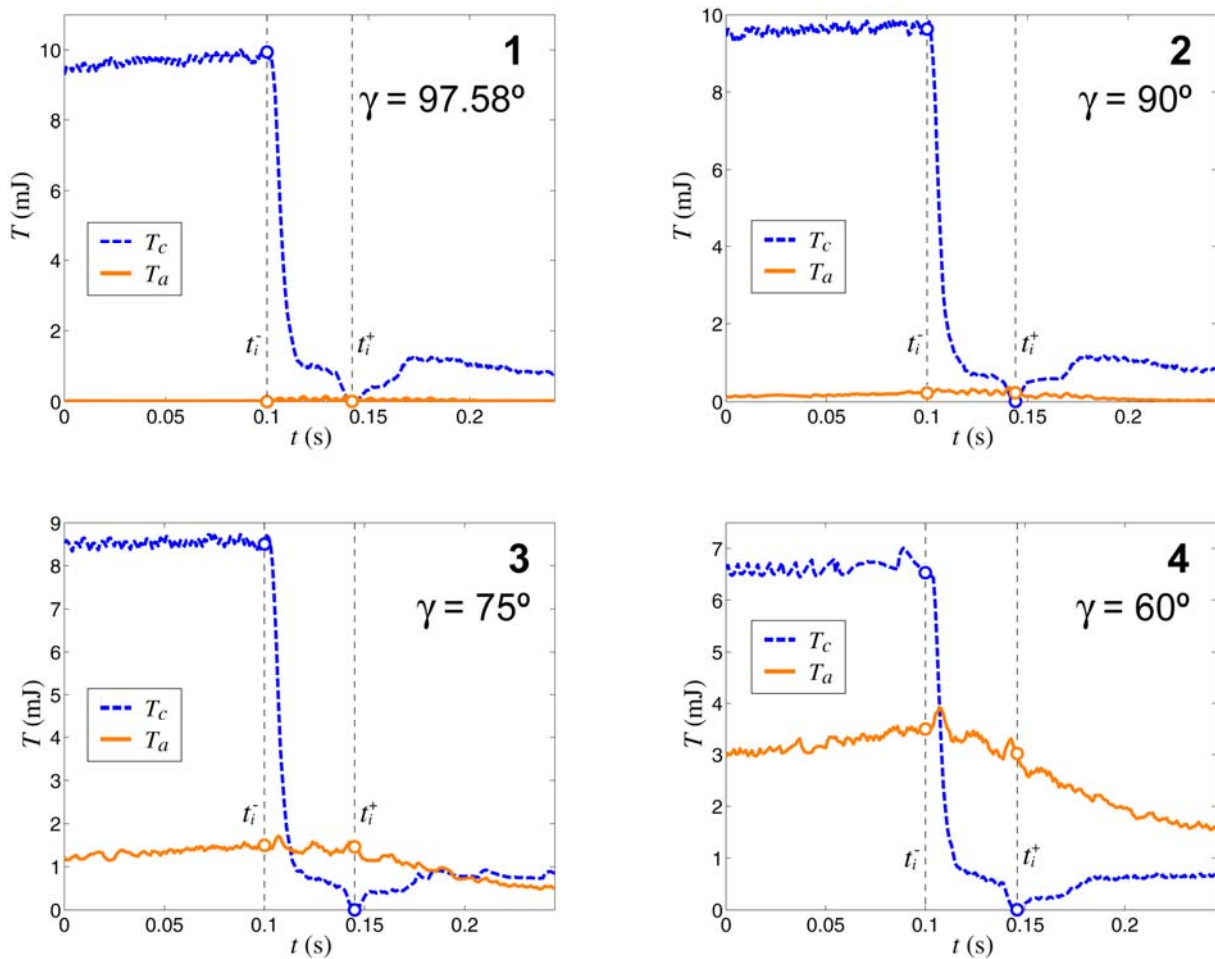


Fig. 5. Kinetic energy decomposition T_c , T_a during one individual experiment for cases 1 to 4.

Table (4) shows the actual measured quantities of the kinetic energy decomposition, the ratio ξ , and the measured impulses $\bar{\lambda}$ and $\bar{\beta}$ at the tip of the active device. These impulses are defined positive with the sense indicated in Fig. (4b). The first represents the impulse of the normal contact force associated with the constraint, whereas the second denotes the impulse of the non-ideal force developed along the tangential direction. The results are in very good agreement with the previous computations in Table (3). Several conclusions can be drawn from them. First of all, we find that the maximum constraint impulse is observed for the case of maximum ratio ξ (case 1). Hence, T_c^- is a good indicator of the magnitude of the constraint forces generated during the transition. As it can be observed, there is a clear correlation between T_c^- and $\bar{\lambda}$.

Table 4. Experimental results for the four cases.

Case	T_c^- (mJ)	T_a^- (mJ)	T_a^+ (mJ)	ξ	$\bar{\lambda}$ (N·ms)	$\bar{\beta}$ (N·ms)
1	9.937	0.001	0.006	1.00	109.57	1.28
2	9.482	0.273	0.223	0.97	105.93	1.40
3	8.506	1.498	1.462	0.85	101.26	0.05
4	6.531	3.490	3.017	0.65	84.97	-2.10

One might expect the most intense contact impulses when the end point velocity is fully aligned with the constrained direction ($\gamma = 90^\circ$). However, we have shown here that this is not generally true in complex multibody systems such as the one considered in this work. It can also be noticed that in general $T_a^+ \neq T_a^-$ due to non-ideal phenomena (e.g., friction) represented by impulse $\bar{\beta}$, that affect the dynamics of the SAM according to Eq. (6). It must be remarked that the largest change in T_a is obtained for case 4 which is the one with the highest tangential impulse. This change can be observed in the corresponding plot of Fig. (5). For cases 1 to 3, the change in T_a is smaller due to lower impulses in the tangential direction.

As for the sign of impulse $\bar{\beta}$, the positive sign for case 1 can be explained because at pre-impact time $\dot{x}_{EE}^- < 0$ (since $\gamma > 90^\circ$) and, therefore, frictional effects are mostly in the opposite sense. Case 2 is not that obvious since for this case we have that $\dot{x}_{EE}^- = 0$, however, the fact that $\bar{\beta} = 1.40$ N·ms implies that there is slipping towards the negative direction of the x axis during the impact interval. In case 3, the measured tangential impulse is positive and almost zero. One could expect a negative value of such impulse because $\dot{x}_{EE}^- > 0$ (since $\gamma < 90^\circ$), however, the measured value implies that slip reversal takes place during the compression phase interval $[t_i^-, t_i^+]$.

CONCLUSIONS

This work presents a method for the dynamic analysis of variable topology mechanical systems based on the concept of bilateral impulsive constraints. The Jacobian of these constraints can be used to define subspaces of the tangent space of the system, which are termed “space of constrained motion” and “space of admissible motion”. Based on this concept, a complete decoupling of the kinetic energy of the system and the impulsive dynamic equations characterizing the event of topology transition can be obtained. The pre-event decomposition of the kinetic energy gives useful information on how energy is redistributed to establish the constraints.

Two situations that may be characterized with impulsive constraints of that class are explored to illustrate the concepts of the paper. First, the dynamics of the heel strike event in bipedal locomotion is analyzed. The kinetic energy redistribution and the impulses on the foot generated during such event are obtained as functions of design parameters and configuration. This analysis provides guidelines that can be useful for control and design of humanoid robots. Second, a thorough experimental study of impact using an instrumented robotic testbed is also performed. Detailed experimental results that validate the concepts derived from the presented approach are reported.

In this paper, the case of having independent constraints is considered. Nevertheless, there may be practical situations where the constraints generated can depend on each other (redundant constraints). This issue will be further addressed as future work.

ACKNOWLEDGEMENTS

We acknowledge the support of the Natural Sciences and Engineering Research Council of Canada, the Canada Foundation for Innovation, and the Technical University of Catalonia.

REFERENCES

- [1] K.H. Hwang, A.A. Shabana, *Effect of Mass Capture on the Propagation of Transverse Waves in Rotating Beams*, J. Sound Vib., 186 (1995), 495-525.
- [2] S.H. Collins, A. Ruina, R. Tedrake, M. Wisse, *Efficient Bipedal Robots Based on Passive-Dynamic Walkers*, Science, 307 (2005), 1082-1085.
- [3] T. McGeer, *Passive Dynamic Walking*, Int. J. Robotics Research, 9 (1990), 62-82.
- [4] A.D. Kuo, J.M. Donelan, A. Ruina, *Energetic consequences of walking like an inverted pendulum: Step-to-step transitions*, Exercise and Sport Sciences Rev., 33 (2005), 88-97.
- [5] A.D. Kuo, *Energetics of Actively Powered Locomotion Using the Simplest Walking Model*, J. Biomech. Eng., 124 (2002), 113-120.
- [6] L.A. Pars, *A Treatise on Analytical Dynamics*, Heinemann, (1965).
- [7] J. Kövecses, W.L. Cleghorn, *Finite and Impulsive Motion of Constrained Mechanical Systems via Jourdain's Principle: Discrete and Hybrid Parameter Models*, Int. J. Non-Linear Mechanics, 38 (2003), 935-956.
- [8] J. Kövecses. *Dynamics of Mechanical Systems and the Generalized Free-Body Diagram—Part I: General Formulation*, J. Appl. Mech., 75 (2008), 061012, 1-12.
- [9] W. Blajer, *A Geometric Unification of Constrained System Dynamics*, Multibody System Dynamics, 7 (1997), 3-21.
- [10] J.M. Font-Llagunes, J. Kövecses, *Dynamics and energetics of a class of bipedal walking systems*, Mechanism and Machine Theory, 44 (2009), 1999-2019.
- [11] F. Asano, Z.W. Luo, M. Yamakita, *Biped Gait Generation and Control Based on a Unified Property of Passive Dynamic Walking*, IEEE Trans. Robotics, 21 (2005), 754-762.
- [12] M. Kwan, M. Hubbard, *Optimal Foot Shape for a Passive Dynamic Biped*, J. Theoretical Biology, 248 (2007), 331-339.
- [13] V. Duindam, S. Stramigioli, *Optimization of mass and stiffness distribution for efficient bipedal walking*, IEEE Int. Conf. Intelligent Robots and Systems, Edmonton, Canadá, (2005).
- [14] J. Kövecses, J.M. Font-Llagunes, *An Eigenvalue Problem for the Analysis of Variable Topology Mechanical Systems*, J. Computational and Nonlinear Dynamics, 4 (2009), 031006, 1-9.